The effect of grain boundary precipitates on the creep behavior of Inconel 718

W. Chen and M. C. Chaturvedi

Department of Mechanical and Industrial Engineering, University of Manitoba, Winnipeg, Manitoba R3T 2N2 (Canada)

(Received July 20, 1993; in revised form September 22, 1993)

Abstract

Inconel 718 has been heat treated to produce materials with microstructures that have the same distribution of γ''-strengthening precipitates within the grains but with grain boundaries that are either clean or have a nearly uniform distribution of 5 μ δ-Ni_3Nb precipitates. Creep tests on specimens with these two types of microstructures have been conducted in the temperature range of 600–650 °C at constant applied stresses in the range of 745–820 MPa. It is observed that the presence of precipitates at grain boundaries increases the creep rate and its stress exponent. It is suggested that the presence of precipitates on grain boundaries changes the creep mechanism from volume-diffusion controlled to grain-boundary controlled. It is likely that the "constant structure" creep model proposed by Robinson *et al.* is applicable to the material with precipitates on the grain boundaries.

1. Introduction

In the power-law dislocation creep region, it is generally believed that grain boundary sliding takes place only to accommodate the deformation that occurs in the grain interiors. As pointed out by Cadek [1], it is only when the related process of intergranular creep fracture is considered that grain boundary sliding returns to play a centrally important role. In fact, in the last two decades, most of the investigations of grain boundary sliding under dislocation creep conditions have been aimed at its role in intergranular void formation.

The precipitate particles at grain boundaries have been generally assumed [2–5], and occasionally observed [6–8], to inhibit grain boundary sliding. Since only a minor role is played by grain boundary sliding, as far as the overall creep strain and creep rate are concerned, the effect of precipitates at grain boundaries on creep resistance in the dislocation creep region is often ignored [1]. However, it has attracted some attention recently [9–11]. For example, it has been observed that the apparent stress dependence of creep in Nimonic 80A is significantly influenced by carbide particles present at grain boundaries [9]. More recent investigations on some heat-resistant steels have revealed that their creep resistance is improved by an order of magnitude [10, 11] by the presence of precipitates at grain boundaries. Such results seem to be inconsistent with the assumption that only a minor role is played by grain boundaries in the dislocation creep region. Therefore, studies have been initiated to examine the role of grain boundary precipitates on creep deformation of two-phase materials. In a previous study on Inconel 718 [12], it was observed that there exists a range of precipitate particle sizes of the strengthening phase, γ'', over which the creep rate is insensitive to the strength of grain material when Ni_3Nb-δ precipitate particles are present at the grain boundaries. In this communication, the stress dependence of the creep rate of Inconel 718 with and without precipitates at the grain boundaries is reported.

2. Experimental methods

The chemical composition of Inconel 718 used in this study, as determined by Arrow Lab, Wichita, Kansas (USA), is given in Table 1. A 2.54 mm thick sheet of the alloy was cold-rolled to a thickness of 1.4 mm and machined into flat samples with a gauge dimension of 1.3 mm × 5.3 mm × 2.54 mm. The samples were heat-treated in accordance with the scheme illustrated in Table 2, which is based on the work of other investigators [13–15], in order to obtain controlled and specific microstructures. The creep tests were conducted in the 600–650 °C temperature range

0921-5093/94/$7.00
SSDI 0921-5093(93)09442-L

TABLE 1. Chemical composition of Inconel 718 (wt.%)

C	0.03
Fe	19.24
Ni	52.37
Cr	18.24
Al	0.52
Ti	0.97
Mo	3.07
(Nb + Ta)	4.98
Mn	0.007
S	0.007
Si	0.30
Cu	0.04

TABLE 2. Heat treatment methods used for Inconel 718

Material A	1020 °C × 4 h → R.T. (A.C.), 725 °C × 25 h → R.T. (A.C.)
Material B	1020 °C × 4 h → 725 °C (F.C.), 925 °C × 1 h → R.T. (A.C.), 725 °C × 25 h → R.T. (A.C.)

R.T.: room temperature; A.C.: air cooling; F.C.: furnace cooling.

at applied stresses in the range of 745–820 MPa on Denison constant stress creep machines. The test temperature was controlled within ± 3 °C and a flow of argon through the test chamber was maintained. Creep strain was measured using linear variable differential transducers (LVDTs) and was recorded continuously using a strip chart recorder. The consecutive stress reduction method [16–20] was used to determine the back stress during dislocation power-law creep.

The heat-treated as well as creep-deformed specimens were examined by a JEOL 840 analytical scanning electron microscope (SEM) and a JEOL 2000FX analytical transmission electron microscope (TEM). The precipitate particle size was measured by using enlarged micrographs on a Leitz Image Analyzer. Each of these enlarged micrographs contained more than 100 particles. A total of five enlarged micrographs of each material were analyzed. The size of the oblong particles was measured along the longest direction as well as the shortest direction. The value along the long direction represents the diameter of the γ'' discs. Creep tests on some samples were interrupted and creep specimens were cooled by pressurized air. These specimens were used to examine the microstructures of creep-deformed specimens.

3. Results and discussion

3.1. Microstructures before creep testing

Figure 1 is a TEM image of material A showing clean grain boundaries obtained by air cooling after solid solution treatment at 1020 °C for 4 h. Material B was furnace-cooled from the solution heat treatment temperature of 1020 °C, which produced coarse precipitates of $\gamma'' + \gamma'$ phases in the grain interiors as well as smaller particles of δ-phase (about 0.4 μm) at grain boundaries (Fig. 2(a)) [13–15]. The second solid solution treatment of this material at 925 °C for 1 h was designed to dissolve $\gamma'' + \gamma'$ precipitates within the grain interiors and maintain the δ-phase at grain boundaries without excessive coarsening (Fig. 2(b)) [15]. The aging of both materials A and B at 725 °C for 25 h produced γ'' and γ' precipitate particles in the grain interiors as illustrated in Figs. 3(a) and 3(b). The diameter of the γ'' discs was quantitatively determined to be 16.7 nm in material A and 17.3 nm in material B. The size of δ precipitates at the grain boundaries in material B was about 5 μm. The final grain size of both materials A and B was found to be about 59 μm. Therefore the material heat treated in accordance with the scheme described in Table 2 produced similar sized grains and strengthening precipitate particles within the grain interior of both the materials. The only difference was at the grain boundaries; material B had δ precipitates at the grain boundaries, whereas the grain boundaries of material A were precipitate-free.

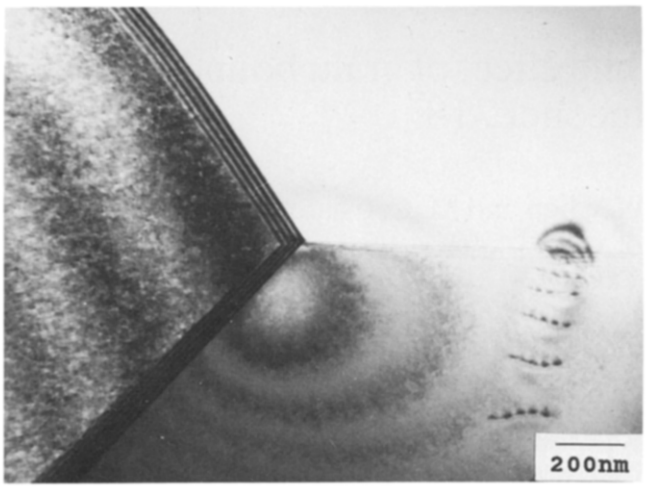

Fig. 1. TEM image showing clean grain boundaries in material A.

3.2. Stress dependence of creep rate

Specimens of both materials A and B were creep tested at 625 °C. Typical creep curves for both materials A and B are shown in Fig. 4, which were obtained when tests were conducted at an applied stress of 770 MPa. Figure 5 shows the variation in creep rate with creep testing time observed in both materials tested at various stress levels. It is observed that the creep rate *vs.* time plot of material A (Fig. 5(a)), which has precipitate-free grain boundaries, exhibits a minimum in

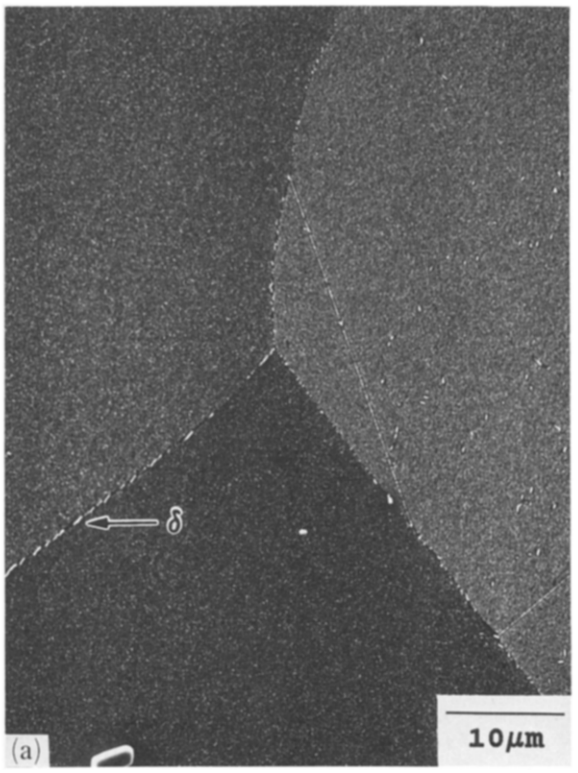

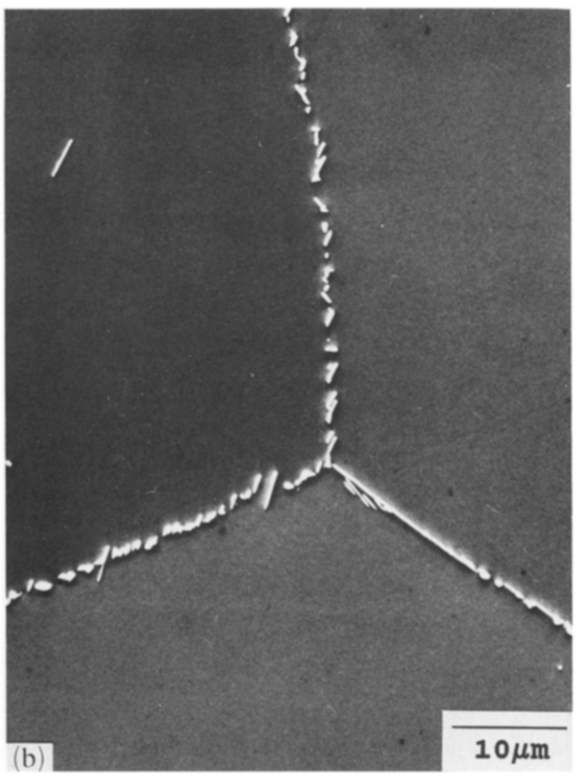

Fig. 2. SEM images showing precipitates at grain boundaries in material B: (a) after furnace cooling from solid solution treatment at 1020 °C; (b) after partial solid solution treatment at 925 °C.

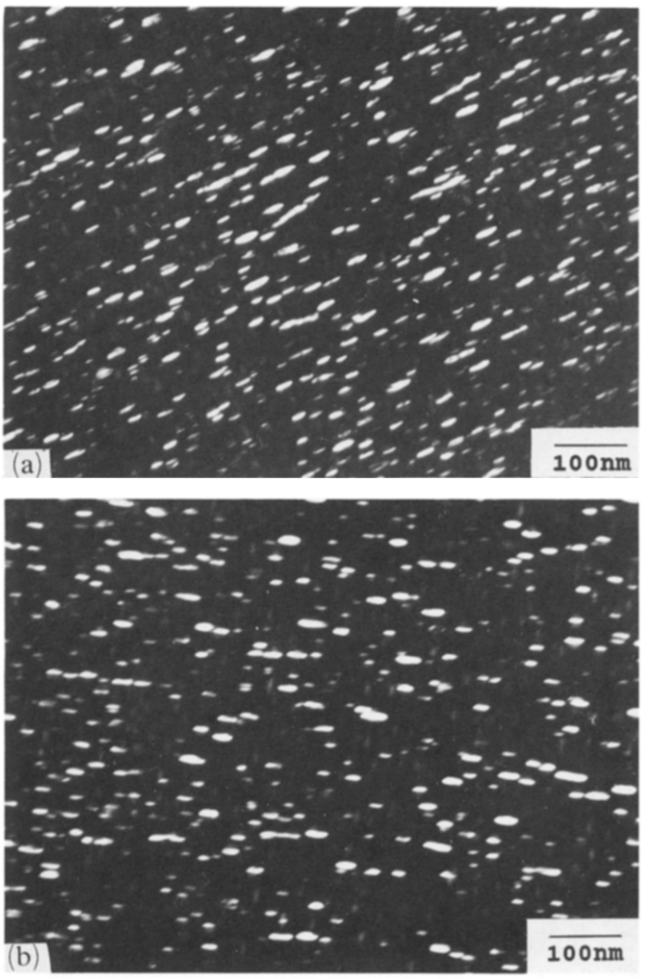

Fig. 3. TEM images showing precipitates of γ'' in material A (a) and material B (b).

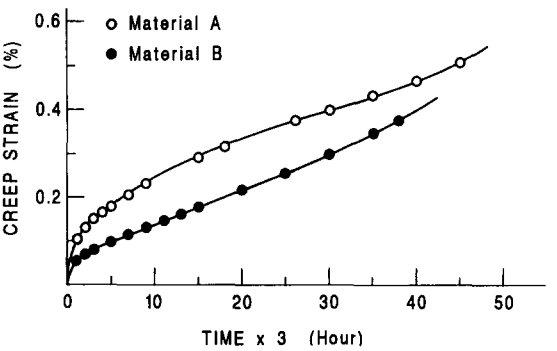

Fig. 4. Creep strain-time curve for materials A and B tested at 625 °C and at a stress of 770 MPa.

creep rate, while a steady-state creep rate stage is observed in the plots obtained for material B at every level of applied stress (Fig. 5(b)). Besides the steady-state stage, a specimen of material B tested at 745 MPa also shows a minimum in the creep rate–time plot. The

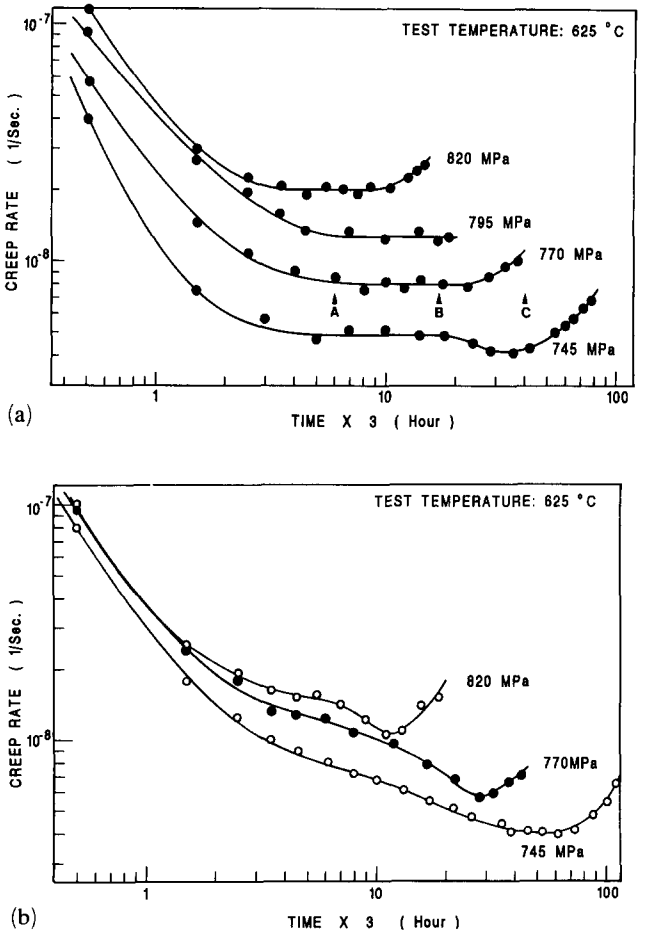

Fig. 5. (a) Creep curve for material A (clean grain boundaries). (b) Creep curve for material B (δ-precipitates at grain boundaries).

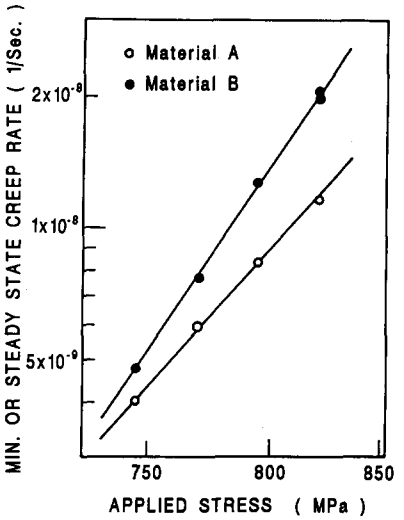

Fig. 6. Dependence of creep rate on applied stress at 625 °C.

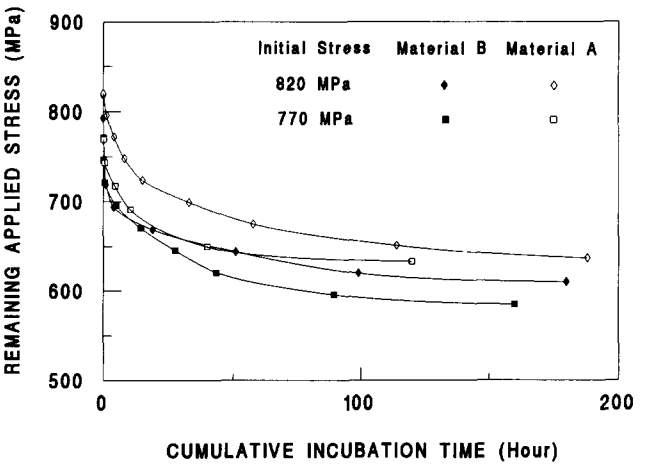

Fig. 7. Relationship between cumulative incubation time and remaining applied stress.

minimum creep rate values and the steady-state creep rate values have been plotted against the applied stress in Fig. 6. It is seen that, at a given value of applied stress, material B, with δ precipitates on the grain boundaries, has a higher value of steady-state creep rate compared with the minimum creep rate oberved in material A. The apparent stress dependence of creep rate for material B is also somewhat higher than that of material A, *i.e.* the value of apparent stress exponent n_a is 13 for material B and 11 for material A.

These high values of stress exponent are similar to those observed in two-phase materials [21]. In these materials creep deformation occurs under the influence of an effective stress, which is given by $(\sigma_a - \sigma_b)$. In this expression, σ_a is the applied stress and σ_b is the back stress. The consecutive stress reduction method [16–20] was employed to determine the back stress σ_b for both materials during creep testing. An incubation period after about 5% stress reduction was observed in both materials. Figure 7 shows some examples of the relationship between the cumulative incubation time and residual applied stress for both the materials tested at 625 °C and at initial applied stress of 820 MPa and 770 MPa. The values of back stresses obtained experimentally are plotted against the initial applied stress in Fig. 8. It is seen that the back-stress values obtained at all the initial applied stress levels are much higher in material A with clean grain boundaries than those observed in material B with δ-precipitates at the grain boundaries. It should also be noted that the value of back stress for material A is not influenced significantly by the values of initial applied stress. This observation is similar to the results reported earlier [22, 23] on Inconel 718 with clean grain boundaries but with a γ'' strengthening precipitate size of 26.9 nm. However, the value of back stress for material with δ precipitates at the grain boundaries increased from 578 MPa to 607 MPa when the initial applied stress is increased from 745 MPa to 820 MPa.

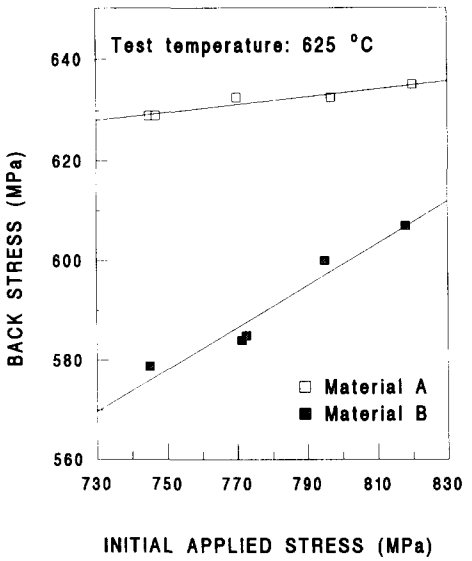

Fig. 8. Dependence of back stress on applied stress at 625 °C.

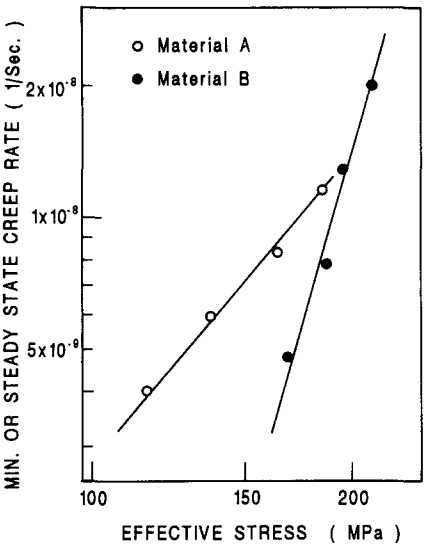

Fig. 9. Dependence of minimum or steady-state creep rate on effective stress.

The effective creep stress, σ_e, which is obtained by subtracting the back stress from applied stress is plotted against minimum creep rate for material A and steady-state creep rate for material B in Fig. 9. The values of the effective stress exponent of creep rate were calculated from these plots. The value of n_e for material A was found to be 3.0. This is similar to values normally observed in two-phase materials that follow the dislocation power law creep mechanism based on interaction of dislocations with obstacles within the grain interior [21, 24]. The value of $n_e = 6.8$ for material B is higher than that normally observed for two-phase materials. This would suggest that the creep mechanism operating in material B is different than that operating in material A.

3.3. Activation energy for the creep deformation process

The activation energy for the deformation process is a reflection of the mechanism of creep deformation. Therefore, the activation energies were measured for both materials.

The creep strain rate, $\dot{\varepsilon}_s$, applied creep stress, testing temperature T, and apparent activation energy, Q_a, are related by the following creep rate equation:

$$\dot{\varepsilon}_s = A\left(\frac{\sigma_a}{G}\right)^{n_a}\left(\frac{Gb}{kT}\right)\exp\left(-\frac{Q_a}{kT}\right) \tag{1}$$

where n_a is the apparent stress exponent, G is the shear modulus, b is the Burger's vector, k is the Boltzmann constant and A is a material constant.

The apparent activation energy, Q_a, can be obtained from the slope of the plot of $\ln(\dot{\varepsilon}_s T/G)(G/\sigma_a)^{n_a}$ *vs.* $1/T$. Therefore, both the materials were tested at 600 °C and 650 °C at an applied stress of 820 MPa. The $\ln(\dot{\varepsilon}_s T/G)(G/\sigma_a)^{n_a}$ *vs.* $1/T$ plots are shown in Fig. 10. The calculated values of apparent activation energy, Q_a, listed in Table 3, (450–475 kJ mol^{-1}) are much higher than those observed for self-diffusion or for the creep process in pure nickel and Ni–Cr solid solution (265–295 kJ mol^{-1}) [25, 27]. However, eqn. (1) does not consider the influence of back stress on the creep rate and the activation energy. Therefore, the creep rate equation is modified as follows by replacing σ_a by $(\sigma_a - \sigma_b)$ [20].

$$\dot{\varepsilon}_s = A\left(\frac{\sigma_a - \sigma_b}{G}\right)^{n_e}\left(\frac{Gb}{kT}\right)\exp\left(-\frac{Q_e}{RT}\right) \tag{2}$$

From this expression, the effective activation energies, Q_e, can be determined from the slopes of $\ln(\dot{\varepsilon}_s T/G)[G/(\sigma_a - \sigma_b)]^{n_e}$ *vs.* $1/T$.

The back stress of Inconel 718 with clean grain boundaries is shown to decrease with an increase in temperature [22, 23]. This was confirmed in the present study; the back stress for both the material with clean grain boundaries and the material with δ precipitates on the grain boundaries was observed to decrease with an increase in temperature, as shown in Fig. 11. The $\ln(\dot{\varepsilon}_s T/G)[G/(\sigma_a - \sigma_b)]^{n_e}$ *vs.* $1/T$ plots, using temperature-corrected values of σ_b, are shown in Fig. 12. From these plots, the effective activation energy was determined to be 248.1 and 250.8 kJ mol^{-1} respectively for material A and material B, and are listed in Table 3. These values are in reasonable agreement with the activation energies observed for self-diffusion and for creep deformation of pure nickel and Ni–Cr solid solution alloys (265–295 kJ mol^{-1}) [25–27]. These

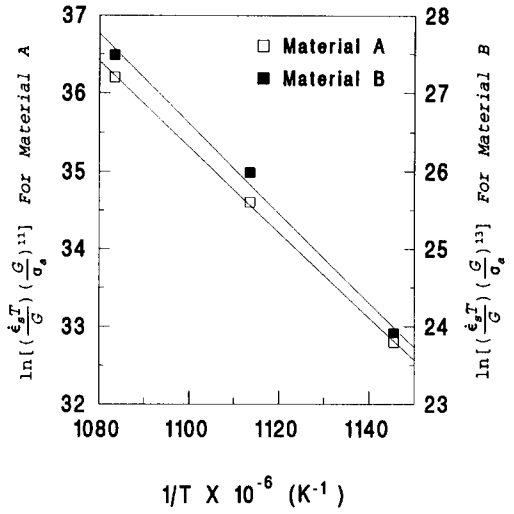

Fig. 10. Determination of the value of apparent activation energy.

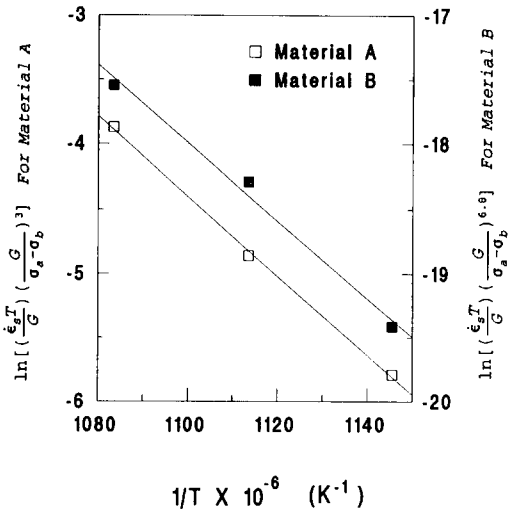

Fig. 12. Determination of the values of effective activation energy.

TABLE 3. Experimentally determined activation energy of creep

Material	Q_a (kJ mol^{-1})	Q_e (kJ mol^{-1})
Material A	452.7	248.1
Material B	473.6	250.8
Pure Ni and Ni–Cr alloys	265–295 [25–27]	

Q_a: Apparent activation energy.
Q_e: Effective activation energy.

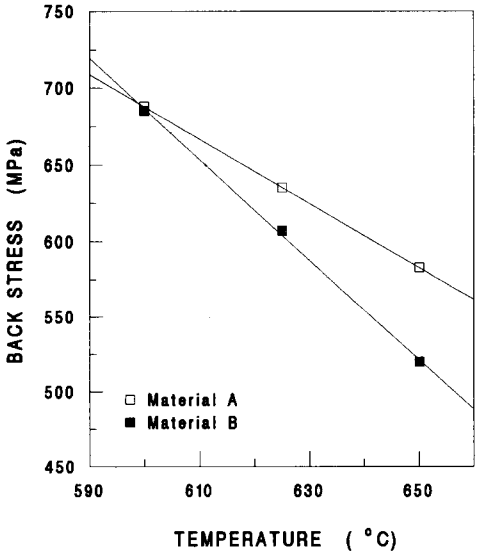

Fig. 11. Effect of temperature on back stress at the initial applied stress of 820 MPa.

values of Q_e suggest that the creep deformation process in both materials is thermally activated and involves vacancy migration [22–24].

3.4. *Microstructures after creep deformation*

The microstructures of specimens of both materials creep tested to failure at 625 °C were examined by TEM and SEM. It was found that no coarsening of the grain boundary or grain interior precipitates occurred during the creep tests in either of the two materials. For example, the size of γ'' precipitates present in the grain interior and δ precipitates present at the grain boundaries in the specimen of material B tested at 625 °C and at a stress of 770 MPa shown in Figs. 13(a) and 13(b) are similar to that observed in undeformed specimens (Figs. 3 and 2(b)). Coarsening probably does not occur because the testing temperature of 625 °C is below the heat treatment temperature at which the original microstructures were produced, and therefore, the microstructures did not change over the duration of the test to any significant extent [13].

Void formation at the grain boundaries can also influence the creep behaviour. Therefore, the microstructures of creep-tested specimens were also examined to determine if voids form at the grain boundaries during creep deformation. Voids were not observed in specimens of material A creep deformed up to failure. Instead wedge cracks were often observed which would be responsible for the creep failure of the material. However, they were observed in specimens of material B that had undergone significant creep deformation. For example, the grain boundaries of a specimen deformed to position A marked in Fig. 5(b), which is a creep curve of a specimen tested at 625 °C and at a

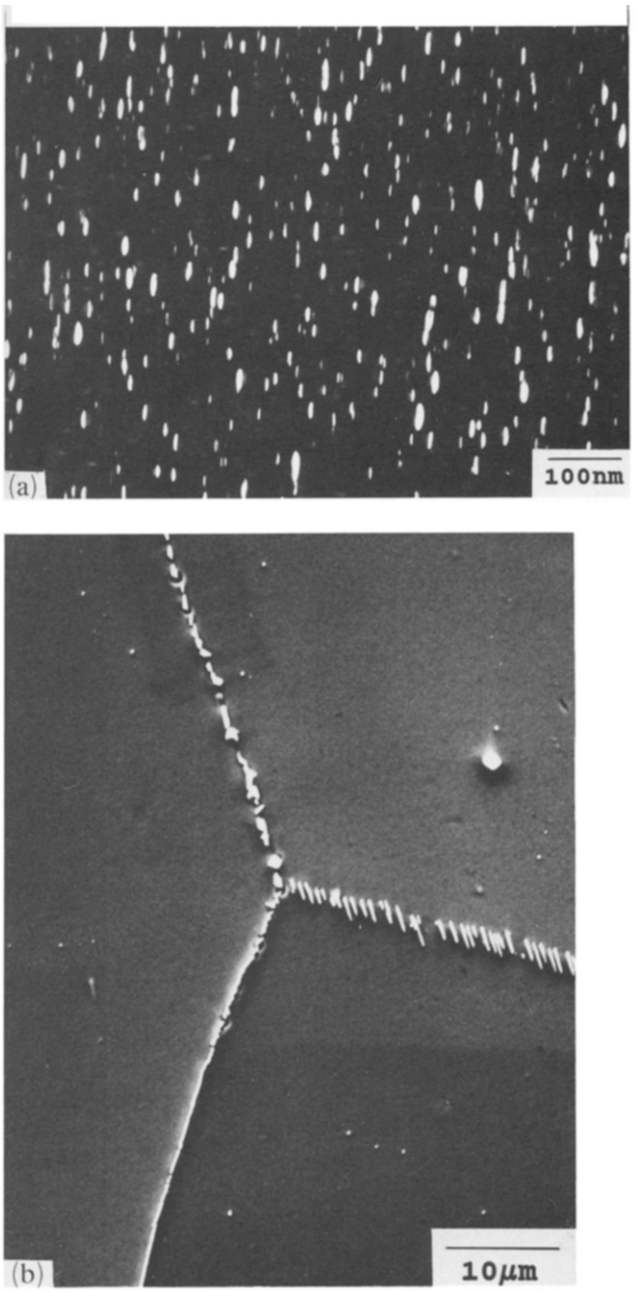

Fig. 13. Microstructures of material B after creep test at 625 °C and an applied stress of 770 MPa: (a) γ''-precipitates in grain matrix; (b) δ-precipitates at grain boundaries.

stress of 770 MPa, were free of any voids, as shown in Fig. 14(a), which is an enlarged SEM image of δ precipitates at a grain boundary. However, when this specimen was deformed to stage marked B, which is towards the end of steady-state creep stage, small isolated creep voids around δ precipitate particles were occasionally observed, as shown in Fig. 14(b). In the tertiary stage (position C), a significant number of voids were observed as seen in Fig. 14(c). The presence of these voids would explain the rapid rise in the creep rate during the tertiary stage of deformation.

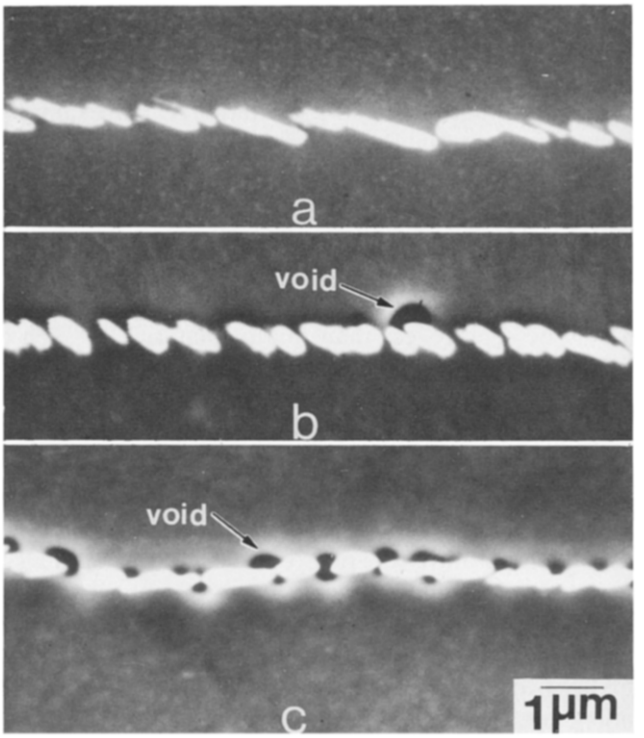

Fig. 14. Microstructures of grain boundaries in material B. The material has been tested and interrupted at (a) position A, (b) position B, and (c) position C as in Fig. 5(b).

3.5. The role of grain boundary precipitates in creep deformation

In the power-law dislocation creep region, grain boundary sliding can make some contribution to the overall creep deformation of a material, especially at low applied stresses. The upper limit of this contribution has been calculated to be $(1.4)^n$ over that contributed by the creep deformation of the grain material [28]. In this factor, n is the stress exponent. It has also been observed that the value of n is the same whether or not grain boundary sliding makes a significant contribution to the overall amount of creep deformation [28, 29]. Grain boundary sliding should be inhibited by the presence of precipitates on the grain boundaries [2–8]. Therefore, the contribution of grain boundary sliding to the total creep deformation and the creep rate should be reduced by the presence of grain boundary precipitates as has been observed in the materials [2–8]. However, the results presented in this communication show that the creep resistance of material B, with precipitates on the grain boundaries, is less than that of material A with clean grain boundaries. That is, the presence of precipitates on the grain boundaries has actually reduced the creep strength of this material. This is also reflected in a significant reduction in the value of the back stress of material B compared with that of material A. Such a reduction in

the value of back stress has increased the value of effective stress at a given value of applied stress and the value of effective stress exponent, n_e, is significantly higher than that observed in material A. For example, $n_e = 6.8$ for material B and $n_e = 3.0$ for material A.

The formation of boundary precipitates in material B may cause a slight reduction in the volume fraction of γ'' precipitates within the grains. Therefore, although the size of the strengthening precipitate, γ'', is the same within both materials A and B, the strength of material B may be slightly less than that of material A. Such a reduction in strength may reduce the creep strength and back stress of material B. To evaluate this aspect, both materials A and B were tensile tested at 625 °C. The 0.2% yield stress of material A was observed to be 806 MPa and that of material B was 816 MPa. That is, the yield stress of both the materials at the creep-testing temperature was nearly the same. It should also be noted that even if the yield stress of material B was somewhat less than that of material A, it cannot explain the strong dependence of the back stress of material B on applied stress compared with the almost stress independence of the back stress of material A (Fig. 8). Therefore, a slight reduction in the volume fraction of γ'' precipitates in material B cannot explain the difference in creep behavior of the two materials. Instead, it would seem that the presence of δ precipitates at the grain boundaries in this material changes the creep mechanism from one of volume controlled to that of grain boundary controlled. In this regard, Sherby's "constant structure" creep model deserves consideration [30, 31]. The applicability of this model to material B is considered next.

The effective stress exponent of material A, $n_e = 3.0$, suggests that the creep mechanism is based on the interaction of dislocations with individual barriers within the grains [24]. These barriers are γ'' precipitate particles. In material B, the value of $n_e = 6.8$ is much higher than that of material A. This value is also higher than the normally reported values in the range 3–5 for power-law creep. A similarly larger value of stress exponent for materials where subgrains form during creep, has been explained by Robinson *et al.* on the basis of the "constant structure" creep model [30, 31]. This model has also been supported by many other investigators [32–35]. According to this model, when subgrains form during creep deformation, the creep rate is influenced by the subgrain size. Robinson *et al.* [30, 31] proposed the following expression to incorporate the influence of subgrain size on the steady-state creep rate:

$$\dot{\varepsilon}_s = S\left(\frac{D_{Eff}}{b^2}\right)\left(\frac{\lambda}{b}\right)^p\left(\frac{\sigma}{E}\right)^N \tag{3}$$

where S is a microstructural constant dependent upon the stacking fault energy and dislocation structure, D_{Eff} is the effective diffusion coefficient, b is the Burger's vector, exponents N and p are constant, and λ is the subgrain size. The value of λ is stress-dependent and can be expressed as $\lambda \propto (\sigma/E)^{-1}$. By substituting this in eqn. (3), the creep rate equation becomes:

$$\dot{\varepsilon}_s = S'\left(\frac{D_{eff}}{b^{2+p}}\right)\left(\frac{\lambda}{b}\right)^p\left(\frac{\sigma}{E}\right)^{N-p} \tag{4}$$

The value of p has been found to be nearly equal to 2. That is, the stress exponent of the creep rate of materials that form the subgrain during creep deformation is nearly equal to $n = N - 2$. In material B, creep deformation is controlled by the grain boundary microstructure because its grain microstructure is otherwise the same as that of material A. Therefore, if grain boundaries in material B were considered to be equivalent to subgrains in their influence on creep deformation, the value of n_e will be reduced to 4.8 from $n_e = 6.8$, which is within the range of values observed in two-phase materials. This would suggest that the presence of δ precipitates at the grain boundaries in Inconel 718 has changed the creep mechanism from grain-controlled to grain-boundary-controlled. Further research is being continued to determine the applicability of Robinson *et al.* "constant structure" creep model to this material.

4. Summary and conclusions

The effect of δ precipitates on the creep deformation of Inconel 718 has been studied. Specimens with the same grain size and γ'' precipitates, but with either precipitate-free grain boundaries or with 5 μm δ grain boundary precipitates have been creep deformed at stresses in the range of 745–820 MPa and at temperatures in the range of 600–650 °C. The results suggest that:

(1) Material with precipitates on the grain boundaries has a higher creep rate than material with clean grain boundaries.

(2) The back stress of material with precipitates on the grain boundaries is also smaller and is significantly dependent upon the applied stress.

(3) The values of effective activation energies for the creep deformation process are nearly the same as that observed for self-diffusion in nickel and nickel–chromium solid solution.

(4) The value of the effective stress exponent of creep rate for clean grain boundary material is observed to be 3.0, which is in the same range as generally observed for other two-phase alloys. However, for material with grain boundary precipitates, the value of n_e is observed to be 6.8, which is considerably higher

than the generally observed value. This high value of n_c can be explained on the basis of the "constant structure" creep model of Robinson *et al.*

Acknowledgments

The authors would like to thank the Natural Science and Engineering Research Council of Canada for financial support and to the University of Manitoba for the award of a graduate fellowship to W. Chen.

References

1 J. Cadek, in *Creep in Metallic Materials*, Materials Science Monographs 48, Elsevier, New York, 1988, p. 270.
2 H. J. Murphy, C. T. Sims and G. R. Heckman, *Trans. Metall. Soc. AIME, 239* (1967) 1961.
3 C. T. Sims, in B. H. Kear, D. R. Muzyka, J. K. Tien and S. D. Wlodek (eds.), *Superalloys: Metallurgy and Manufacture, Proc. 3rd Int. Symp.*, Claitor's Publishing, Baton Rouge, LA, 1976, p. 1.
4 W. Betteridge and A. W. Franklin, *J. Inst. Met., 85* (1957) 473.
5 H. E. Collins, *Metall. Trans., 5* (1975) 187.
6 Ye. Ye. Levin and B. M. Gugelev, *Fiz. Met. Metalloved., 28* (5) (1969) 921.
7 C. A. P. Horton, *Acta Metall., 20* (1972) 477.
8 C. A. P. Horton, *Scr. Metall., 8* (1974) 1.
9 F. T. Furillo, J. M. Davidson, J. K. Tien and L. A. Jackman, *Mater. Sci. Eng., 39* (1979) 267.
10 T. Matsuo, K. Nakajima, Y. Terada and M. Kikuchi, *Mater. Sci. Eng., A146* (1991) 261.
11 J. S. Zhang, P. E. Li, W. X. Chen and J. Z. Jin, *Scr. Metall., 23* (1989) 547.
12 W. Chen and M. Chaturvedi, *Can. Metall. Quart., 32* (4) (1993) 363.
13 A. Oradei-Basile and J. F. Radavich, in E. A. Lotia (ed.), *Proc. Int. Symp. on the Metallurgy and Applications of Superalloys 718, 625 and Various Derivatives, Pittsburgh, PA, June 23–26, 1991*, p. 326.
14 E. Campo, C. Turco and V. Catena, *Metall. Sci. and Tech., J. TEKSID, Italy, 3* (1) (1985) 16.
15 A. K. Koul, P. Au, N. Bellinger, R. Thamburaj, W. Wallace and J.-P. Immarigeon, in S. Reichman, D. N. Duhl, G. Maurer, S. Antolovich and C. Lund (eds.), *Superalloys 1988*, The Metallurgical Society, 1988, p. 3.
16 P. W. Davies, G. Nelines, K. B. Williams and B. Wilshire, *J. Met. Sci., 7* (1973) 87.
17 J. D. Parker and B. Wilshire, *J. Met. Sci., 12* (1978) 453.
18 D. Sidy and B. Wilshire, *J. Met. Sci., 3* (1969) 56.
19 K. R. Williams and B. Wilshire, *Met. Sci., 17* (1983) 145.
20 J. C. Gibling and W. D. Nix, *Mater. Sci. Eng., 45* (1980) 123.
21 R. W. Evans and B. Wilshire, in *Creep of Metals and Alloys*, The Institute of Metals, 1985, p. 106.
22 Y. Han and M. C. Chaturvedi, *Mater. Sci. Eng., 85* (1987) 59.
23 Y. Han and M. C. Chaturvedi, *Mater. Sci. Eng., 89* (1987) 25.
24 G. S. Ansell and J. Weertman, *Trans. AIME, 215* (1959) 838.
25 R. W. Lund and W. D. Nix, *Acta Metall., 24* (1976) 469.
26 J. P. Dennison, R. J. Llewellyn and B. Wilshire, *J. Inst. Metal., 95* (1967) 115.
27 D. Sidy and B. Wilshire, *J. Met. Sci., 3* (1969) 56.
28 W. Beere, *Met. Sci., 16* (1982) 223.
29 F. W. Crossman and M. F. Ashby, *Acta Metall., 23* (1975) 425.
30 S. L. Robinson and O. D. Sherby, *Acta Metall., 17* (1969) 109.
31 C. M. Young, S. L. Robinson and O. D. Sherby, *Acta Metall., 23* (1975) 633.
32 J. C. Gibling and W. D. Nix, in R. C. Gifkins (ed.), *Proc. 6th Int. Conf. on the Strength of Metals and Alloys*, Pergamon Press, Oxford, 1982, p. 613.
33 I. Ferreire and R. G. Stang, *Acta Metall., 31* (4) (1983) 585.
34 G. S. Nakayama and J. C. Gibeling, *Acta Metall., 38* (10) (1990) 2023.
35 K. Milicka, *Acta Metall., 41* (4) (1993) 1163.